Taylor & Francis
Taylor & Francis Group

International Journal of Hyperthermia

ISSN: 0265-6736 (Print) 1464-5157 (Online) Journal homepage: https://www.tandfonline.com/loi/ihyt20

Optimization and characterization of a novel internally-cooled radiofrequency ablation system with optimized pulsing algorithm in an *ex-vivo* bovine liver

Eliel Ben-David, Isaac Nissenbaum, Svetlana Gurevich, Eric R. Cosman Jr & S. Nahum Goldberg

To cite this article: Eliel Ben-David, Isaac Nissenbaum, Svetlana Gurevich, Eric R. Cosman Jr & S. Nahum Goldberg (2019) Optimization and characterization of a novel internally-cooled radiofrequency ablation system with optimized pulsing algorithm in an *ex-vivo* bovine liver, International Journal of Hyperthermia, 36:2, 81-88, DOI: 10.1080/02656736.2019.1617901

To link to this article: https://doi.org/10.1080/02656736.2019.1617901

Published online: 20 Sep 2019.

INTERNATIONAL JOURNAL OF HYPERTHERMIA
2019, VOL. 36, NO. 2, 81–88
https://doi.org/10.1080/02656736.2019.1617901

Taylor & Francis
Taylor & Francis Group

Optimization and characterization of a novel internally-cooled radiofrequency ablation system with optimized pulsing algorithm in an *ex-vivo* bovine liver

Eliel Ben-David[a], Isaac Nissenbaum[b], Svetlana Gurevich[b], Eric R. Cosman Jr[c] and S. Nahum Goldberg[b]

[a]Department of Radiology, Shaare Zedek Medical Center, Jerusalem, Israel; [b]Department of Radiology, Hadassah Hebrew University Medical Center, Jerusalem, Israel; [c]Cambridge Interventional, Burlington, MA, USA

ABSTRACT

Purpose: To prospectively characterize and optimize radiofrequency energy deposition to determine ideal parameters for achieving large ablation zones.

Materials and methods: An internally-cooled RF system was used to perform 214 ablations in 72 *ex-vivo* bovine livers. Tip exposure (1–5 cm), electrode current (400–2500 mA), and application duration (3–15 min) were systematically varied. A pulsing algorithm optimized efficiency of RF deposition, including initial automatic ramping followed by adjustment in current, in response to changes in tissue impedance. Following the procedure ablation diameter and length were measured, sphericity calculated, and correlated with parameters of energy deposition and tissue temperatures.

Results: Increasing electrode exposure from 1–5 cm produced linear increases in ablation diameter from 1.4 ± 0.1 to 5.3 ± 0.1 cm ($y = 1.1x–0.5$; $R^2 = 0.93$), and length ($y = 1.18x + 0.34$; $R^2 = 0.92$). A sphericity index >0.85 was noted at optimal energy setting for electrode exposures of 1–4 cm. Maximum temperatures post-ablation increased with active tip length from $68.5 \pm 4.9\,^{\circ}C$ to $91.3 \pm 1.5\,^{\circ}C$ in a logarithmic ($y = 0.94\ln(x) - 2.75$; $R^2 = 0.90$) or power relationship between temperature and the resultant ablation diameter ($y = 0.27e^{0.0295x}$; $R^2 = 0.76$). A tight exponential relationship ($y = 0.28x^{0.38;}$ $R^2 = 0.97$) was also observed between total energy deposition and ablation diameter. Finally, a multifactor relationship of the diameter of ablation to electrode tip exposure and the time to first impedance rise was successfully modeled, with a root mean squared error of 1.9 mm and $R^2 = 0.95$.

Conclusion: Large, reproducible, and spherical ablation areas can be achieved with the novel system described, with efficient delivery of RF energy deposited into tissue. These findings may have important clinical relevance in regards to the clinical utility of RF ablation compared to other competitive forms of thermal tumor ablation.

ARTICLE HISTORY
Received 13 February 2019
Revised 29 April 2019
Accepted 7 May 2019

KEYWORDS
Radiofrequency ablation; internally-cooled; optimization; characterization; modeling

Introduction

Radiofrequency (RF) ablation is a well-established and reproducible method for performing percutaneous, minimally invasive, thermal ablation of neoplastic disease [1,2]. Given the relatively small ablation volumes initially reported for monopolar electrodes, many techniques for increasing the size of a radiofrequency coagulation zone have been described, including modification of the applicator to include either internal cooling or the use of multiple or multi-tined electrodes [3,4]. Moreover, several iterative or phasic paradigms for applying RF energy based upon changes in tissue impedance, including pulsed energy deposition, ramping of current, and switching of electrode activation have been reported as a more efficient method for increasing RF energy deposition and/or increasing ablation size [5–7]. Despite these advances, several limitations of RF ablation include prolonged ablation time (particularly in comparison to microwave (MW) ablation [8], heat-sink effect adjacent to blood vessels [9], and tissue charring near the electrode due to elevated temperatures from a steep temperature gradient that induces non-desired carbonization and vaporization [10].

Multiple optimization studies have been performed for RF ablation with the stated goal of increasing ablation size by minimizing the relatively poor energy deposition to tissue thermal conductivity mismatch [11–14]. While these prior studies have demonstrated that additional optimization of RF in terms of size and time are possible, most have noted that technical limitations may have prevented full characterization of RF energy/tissue interactions [3,4]. Specifically, early model generators have been limited in power output, in turn, limiting the size of clinically useful electrodes to no more than 3 cm exposure [15]. Moreover, although pulsing algorithms studies have suggested that more dynamic ramping of energy up and down during the ablation cycle with variable timing of the cooling 'off' period may be useful by potentially contribute to heating efficiency [12], thorough evaluation of an internally cooled RF system has not yet been performed. Here, we used a generator that allows up 2500 mA into 50 Ω output, with a programmable interface

CONTACT Eliel Ben-David elib@szmc.org.il Shaare Zedek Medical Center, Dept. of Radiology, Shmuel Bait St 12, Jerusalem, Israel.

Table 1. Summary of ablation parameters studied.

		Target current I0 (mA)																
Electrode exposure (cm)	Duration (minutes)	100	400	450	500	800	1000	1100	1200	1400	1600	1800	1900	2000	2200	2300	2400	2500
1	3		3				4											
	6		3															
	12		3	3	3		4											
	15		3															
2	3						4											
	6						6											
	12	6				3	4	4	4			4			4			
	15						4											
3	3						4			4		4						
	6						4		4	4	4	4						
	12	3			6		6		6	4	4	4		3	4		4	4
4	3											4						
	6											4						
	12	3					6		4	5	4	4	4	6	4	4	4	4
	15											4						
5	6															4		
	9															4		
	12													4	3	3		13
	Total (*N*) 214																	

The distribution of the 214 ablations, based on tip exposure, duration, and target current is presented.

that enables varied dynamic energy deposition, and based upon this technologic advance, report much fuller characterization of the effect of relevant RF parameters (i.e., active electrode tip exposure, duration of energy application, current range, tissue end temperature, heating factor, initial current output, and time of first pulse) for electrode sizes up to 5 cm using an internally-cooled RF system in *ex-vivo* bovine liver with the stated goal of rapidly achieving large ablation zones. Thus, the aim of our study was to evaluate whether large, reproducible, and spherical ablation areas can be achieved with the novel system described.

Materials and methods

Ablation system

An internally-cooled electrode RF system (Cambridge Interventional CRF System, Burlington, Massachusetts) was used to ablate *ex vivo* liver tissue with varied RF electrode tip exposure (1–5 cm), electrode currents (400–2500 mA), and application duration (3–15 min). A total of 214 *ex vivo* ablations were generated in 72 bovine livers to span the space of clinical utility and device capability with a matrix of parameter combinations (Table 1).

The system comprises an RF generator capable of producing 2500 mA output into 50 Ω, a fluid pump, an internally-cooled electrode system, tubing, cables, and four large ground pads (whose currents were individually measured to ensure none receives greater than 900 mA in order to prevent grounding pad burns) [16]. The overall strategy employed by the RF generator's controller was that of optimizing a pulsing algorithm to maximize efficiency of RF deposition. Briefly, the generator initially automatically attempts to achieve an initial pre-set current (I0) by ramping to this value over up to 30 s. Thereafter, the generator adjusts and pulses the electrode current in response to changes in tissue impedance during the ablation. When impedance was stable for 30 s, the current was increased in 100 mA increments to a maximum current setting (Imax). When impedance rises were encountered, a variable cooling off-time period of no energy deposition was initiated to last at least 20 s after a return to impedance baseline was observed. Additionally, the system reduced the RF current by 100 mA if the preceding pulse lasted less than 10 s (Figure 1).

The electrode system includes a 17 gauge internally-cooled electrode, and a coaxial 15 gauge electrically-insulated metallic cannula through which the electrode is introduced into the tissue. The peristaltic fluid pump circulates chilled water (14–16 °C) at 70 ml/min within an electrode to maintain its temperature at or below 22 °C. The cannula includes a metallic active tip exposure through which the electrode conducts RF current to bodily tissue. An electrode and cannula shaft length of 15 cm was used for these experiments. Ablations were generated with single electrodes. Ablation size was assessed by measuring the dissected ablation cross-section and was correlated to starting and maximum current applied, total energy deposition (calculated as a 'heating factor' representing the time-integrated squared RMS current), the tissue temperature (defined as maximum tip temperature following the procedure), and procedure duration. Ablation length and diameter refer to the ablation's maximal extent in the axial and transverse directions of the electrode, respectively.

Ex vivo *model*

Ablations were generated in fresh *ex-vivo* bovine livers obtained from a local abattoir according to the following protocol. Each bovine liver was placed in a $50 \times 39.5 \times 17\,cm^3$ plastic basin containing normal saline solution (Figure 2). The liver was submerged in the saline bath to 1 cm from its superior surface, with an external stand positioned to hold the electrode in place. Prior to each ablation, liver tissue temperatures ranged between 14.5 and 23.5 °C. Each electrode was inserted under ultrasound guidance (Esaote, Italy) to a vertical depth of at least 4 cm and confirmed to be >3 cm from ducts, blood vessels >3 mm,

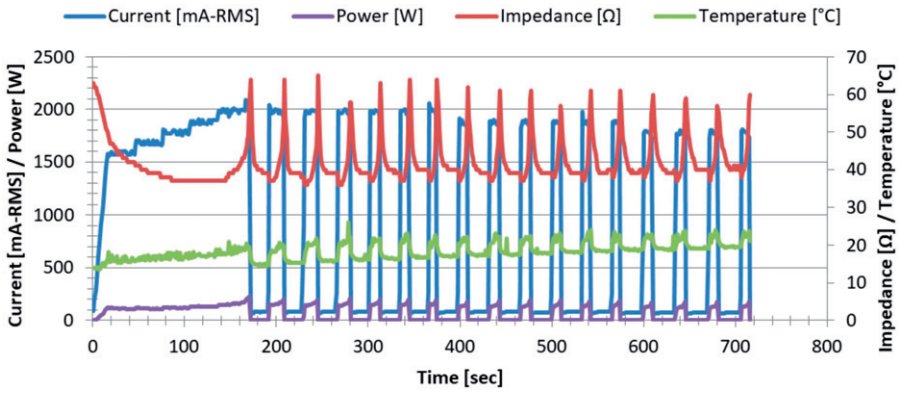

Figure 1. Graphic tracing of a representative course of RF deposition. The tracing demonstrates an initial step-wise increase in energy deposition with periods of cessation of energy deposition following impedance rises. Subsequent step-wise decreases of current are seen when specified energy could not be deposited for 10 s.

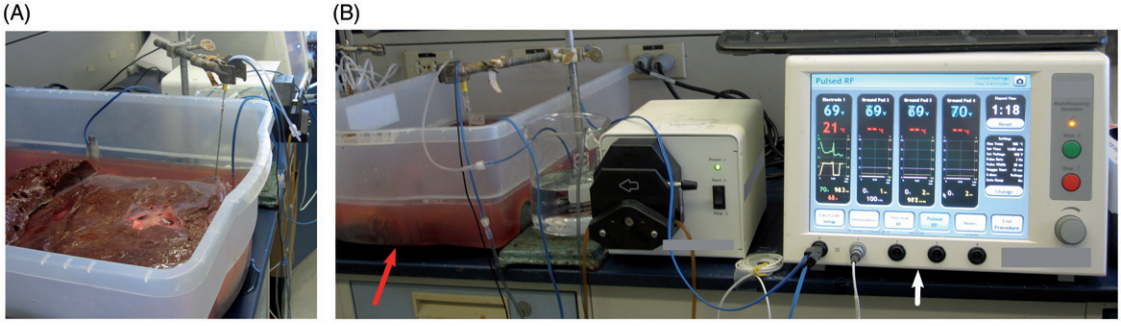

Figure 2. *Ex-vivo* experimental setup. (A) Generator (white arrow) and plastic basin containing saline solution and liver (red arrow). (B) The liver was partially submerged in the saline bath, with a stand holding the electrode in place.

and any tissue surface. Electrode active tip lengths studied included 1, 2, 3, 4, and 5 cm. Ablations for each electrode and settings configuration were performed at least in triplicate. Following each test, the applicator was removed and a needle placeholder was inserted along the long axis of the ablation to allow accurate sectioning of this axis and cross-sectional measurement in two dimensions. The ablations were excised from the tissue at the completion of the ablation with the samples cut with the electrodes remaining *in situ*. The specimens were either cut in the transverse plane to allow for radial measurements of the ablation diameter and/or when noted along the axis of the electrode to visualize a longitudinal cross section of the ablation for length measurements ($N = 45$). Each ablation was photographed with a ruler for scale, and cataloged. All ablations were sectioned, measured, and photographed within one hour of thermal ablation.

Data collection

Data was collected by IN and SNG. Variables studied included electrode exposure, duration of ablation, and target current which were then analyzed for current reached, total energy deposited, tissue end temperature, ablation zone diameter, length, and sphericity index (defined as maximum diameter divided by ablation length). Statistical evaluation was performed by EBD and SNG using paired *t*-tests (SAS Institute, Cary, North Carolina; Excel; Microsoft Corp, Redmond, Washington). Linear and non-linear regression models were formed for fit correlations as appropriate using Microsoft Excel and its GRG Nonlinear Solver Module (Redmond, Washington).

Results

A total of 214 single electrode ablations were generated. The pulsing algorithm worked as intended so that for lower starting currents increases in energy were observed and for higher starting currents (i.e., those that induced impedance rises before achieving the intended target current) a step-wise reduction in energy was automatically implemented that ultimately reached a current level that permitted application of energy for at least 10 s. Thus, the generator was able to quickly optimize the output level to heat tissue efficiently. Moreover, there was a range of ~500 mA of starting current for each electrode exposure size where energy deposition was most efficient, with both this range and the maximum current generally tolerated increasing with tip size (Table 2).

All ablations demonstrated smooth spheroid geometry (Figure 3, Table 3). Configurations that maximize ablation size for a given tip exposure and ablation duration are summarized in Table 2 with representative ablation lengths and the resultant sphericity summarized in Table 3.

Increasing electrode exposure from 1 to 5 cm produced linear increases in ablation diameter ranging from 1.4 ± 0.1 to 5.3 ± 0.1 cm ($y = 1.1x–0.5$; $R^2 = 0.93$), and length ranging from 1.4 ± 0.1 to 6.5 ± 0.4 cm ($y = 1.18x + 0.34$; $R^2 = 0.92$) as

Table 2. Optimal *ex-vivo* settings providing maximum ablation diameter.

Electrode exposure (cm)	*N*=	Duration (min)	Target Current (mA)	Current reached (mA)	Tissue end temperature (C°)	Cross sectional Diameter (cm)
1	3	6	400	700	68.5 ± 4.9	1.4 ± 0.1
1	3	12	400	700	68.5 ± 10.6	1.4 ± 0.2
2	4	6	1000	1300	73.5 ± 1.7	2.4 ± 0.1
2	4	12	1000	1300	71.3 ± 4.9	2.6 ± 0.2
3	4	6	1600	1800	82.5 ± 2.4	3.1 ± 0.1
3	4	12	1800	1900	84.3 ± 1.7	3.4 ± 0.1
4	4	12	1800	2100	88.3 ± 4.3	4.1 ± 0.3
4	4	15	1800	2100	89.8 ± 2.9	4.0 ± 0.2
5	4	12	2500	2500	89.5 ± 1.9	5.0 ± 0.2
5	3	15	2500	2500	91.3 ± 1.5	5.3 ± 0.1

Parameters are presented by electrode exposure size for at least two representative durations of ablation.

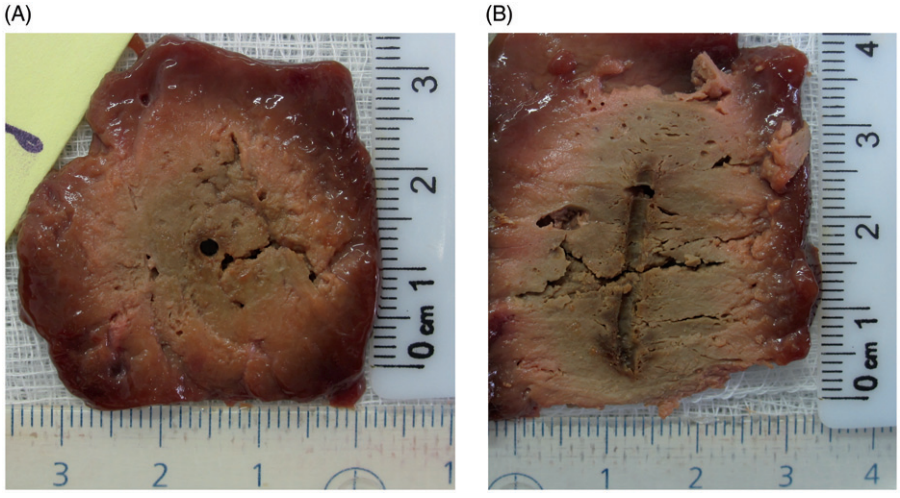

Figure 3. *Ex-vivo* gross pathology. A representative image of the sectioned liver following a six min RF application using a 3 cm single active tip is presented in transverse (A) and axial section (B). White coagulation measuring 2.7 × 2.7 × 3.3 cm is clearly defined.

Table 3. Ablation lengths and sphericity index for 12 min ablation duration.

Electrode Tip exposure (cm)	*N*=	Current range (mA)	Mean (cm)	Range(cm)	Sphericity index
1	5	400–800	1.4 ± 0.1	1.3–1.5	1
2	15	1200–2200	2.8 ± 0.3	2.4–3.3	0.93
3	10	2300–2500	4.0 ± 0.4	3.5–4.7	0.85
4	10	100–2500	5.0 ± 0.5	3.9–5.7	1
5	5	2500	6.5 ± 0.2	6.0–6.9	0.81

detailed in Tables 2 and 3. For each active tip exposure, the generator's initial current setting (I0) did not strongly influence ablation size, over the wide range of setting values studied.

There was no statistical significance ($p \geq .98$) between 6 and 12 min of RF energy deposition for 1 and 2 cm active tips. For 3–4 cm active tip, a 12 min RF application produced greater ablation diameters than 6 min duration ($p < .01$). Yet, increasing duration from 12 to 15 min of heating did not increase ablation diameter for the 4 cm or 5 cm tip exposures ($p > .33$).

Further analysis of the entire data set generated showed two additional strong correlations. First, a power relationship was noted between the maximum electrode temperature immediately after ablation and the resultant ablation diameter ($y = 0.27e^{0.0295x}$; $R^2 = 0.76$), as shown in Figure 4. Moreover, maximum temperatures increased consistently with active tip length from 68.5 ± 4.9 °C for 1 cm to 91.3 ± 1.5 °C for the 5 cm tip exposure. Second, tight logarithmic ($y = 0.94\ln(x)–2.75$; $R^2 = 0.90$) and exponential ($y = 0.28x^{0.38;}$ $R^2 = 0.97$) relationships were also observed between total energy deposition (i.e., the 'heating factor') and the ablation diameter, with maximum heating factors ranging from 88.7 $s*A^2$ for a 1 cm electrode tip exposure to 2903 $s*A^2$ for the 5 cm tip (Figure 5).

When performing sub-analysis based upon electrode tip length, initial current output had only a modest effect on ablation size with R^2 ranging from 0.40–0.70 for the 2–4 cm tip exposures (Figure 6). However, initial currents that were too high resulted in smaller ablation zones. For the longest (i.e., 5 cm) tip exposure, a progressive increase in ablation diameter to 5.3 ± 0.1 cm was seen until the generator reached its maximum current limitation of 2500 mA. By contrast, the smallest, 1 cm tip exposure produced little variability in ablation outcome (0.9 ± 0.1–1.4 ± 0.1 cm diameter), as the current was limited by impedance rises to no more than 800 mA. Figure 7 depicts the correlation between ablation size and time to initial pulse.

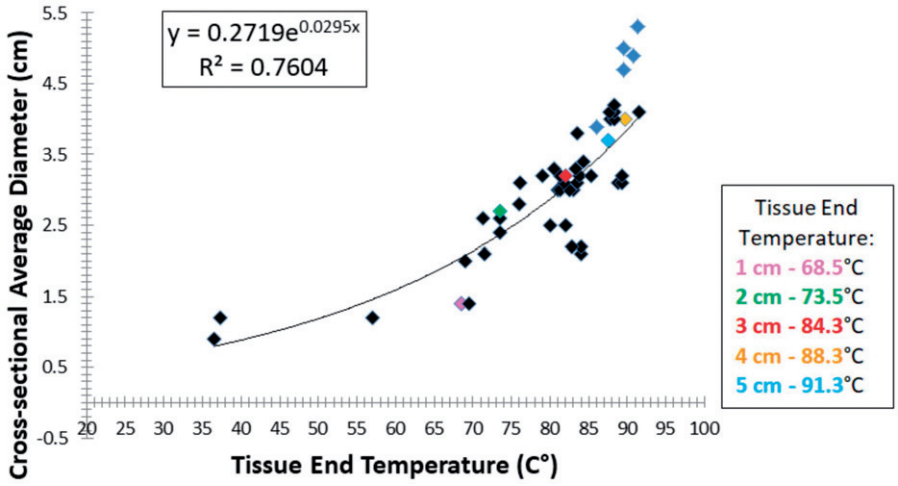

Figure 4. Relationship between maximum electrode temperature immediately after ablation to ablation diameter. A tight correlation to a power function is seen. Colored points represent end temperatures at the optimal settings noted in Table 2.

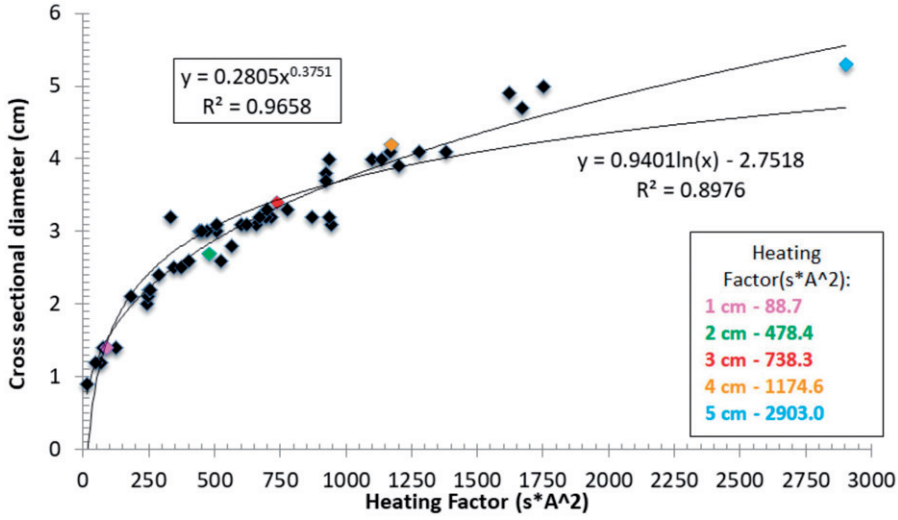

Figure 5. Relationship between 'heating factor' and the ablation diameter. Tight correlations to both power and logarithmic functions are seen. Colored points represent end temperatures at the optimal settings as noted.

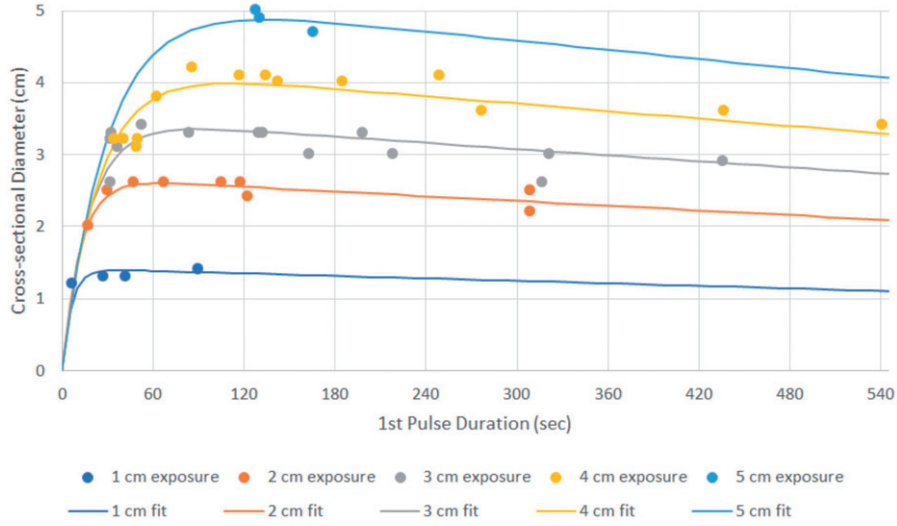

Figure 6. Correlation between initial current output and ablation size. The R^2 for the parabolic correlations observed for 2–4 cm electrode tips and 12 min RF ablation are presented. These results denote that there is a range of optimal initial current which provides the maximum coagulation diameter.

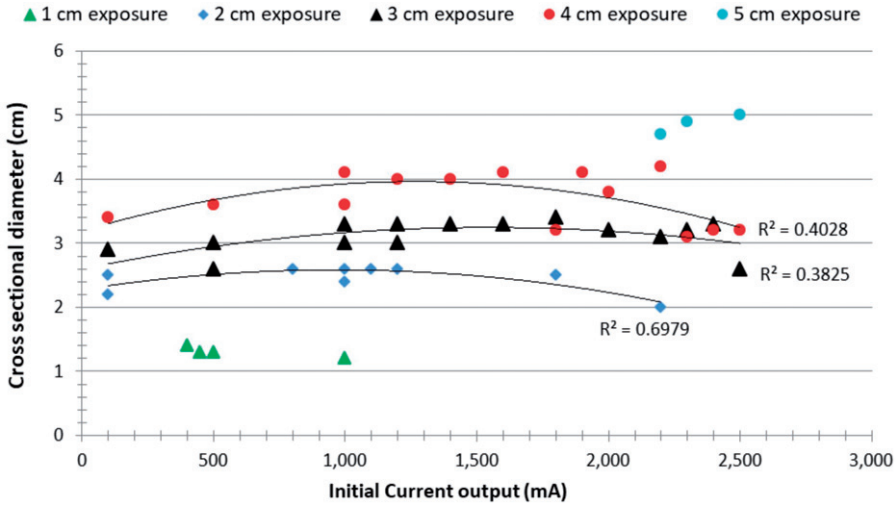

Figure 7. Correlation between the time to first pulse and ablation size. Higher order modeling based upon electrode tip exposure (formula presented in the text) yielded a root mean squared error of 1.9 mm and R^2 of 0.95.

Table 4. Optimized parameters for single-electrode ex vivo data for time to first pulse.

Parameter	Optimized value	Description
D_5	5.222 cm	Ablation scale, 5 cm tip
D_4	4.223 cm	Ablation scale, 4 cm tip
D_3	3.505 cm	Ablation scale, 3 cm tip
D_2	2.680 cm	Ablation scale, 2 cm tip
D_1	1.422 cm	Ablation scale, 1 cm tip
τ	6.018 sec/cm	Time constant
a	2458.859 sec	Time constant

Higher-order modeling of the relationship of the diameter of the ablation to electrode tip exposure and the time to first pulse yielded the tightest correlation to the formula:

$$D = D_L\left(1 - e^{-\frac{t}{\tau L}} - t/a\right)$$

with ablation, width D is modeled as a function of the first-pulse duration t. This yielded a root mean squared error of 1.9 mm and r^2 of 0.95 (Figure 7, Table 4).

This function includes three factors that are influenced by tip length L. The first term (D_L) determines general scale of the ablation for each tip length L. The second term $(1 - e^{-t/\tau L})$ indicates that the ablation width increases rapidly as the first pulse-duration increases from zero (corresponding to a higher-than-optimal and hence counterproductive initial current setting). For a mid-range of initial target currents, ablation diameter reaches a maximum when energy is applied in a range that allows heating for ~30–120 s before inducing the first impedance rise with longer first-pulse durations t noted for longer tip lengths L. The third term (t/a) models the ablation diameters observed when lower initial currents were selected. This reflects diminishing ablation size with longer first-pulse durations.

Discussion

Multiple investigators have demonstrated that non-continuous RF energy application and heating, usually including strategies of pulsing of energy allow for more efficient heat transfer and larger ablation sizes compared to more conventional energy deposition strategies [12]. Ramping of energy has also been shown to be beneficial in increasing RF ablation sizes [17]. Thus, although a balance between heating and cooling has been well known, full exploration of this subject has been lacking.

Our study demonstrates in an *ex vivo* model that with an optimized RF generator, a larger and more spherical zones of ablation can be achieved, most notably when larger tip exposures and greater energy deposition are employed. Indeed, we show a positive correlation between electrode tip size, energy deposition, heating, and ablation outcome correlates with the energy deposition.

Whereas prior studies have noted substantial increases in ablation length and only modest increases in ablation diameter with increased electrode exposure [18], our current study demonstrates that tip length may have greater effect on diameter than previously appreciated. Specifically, we observed that there were increases in diameter as well as increases in sphericity compared to prior reports for 3–5 cm tip exposures. Indeed, the lack of sphericity (i.e., the creation of oblong shaped zones of ablation) has been reported as an issue for many RF and microwave systems [19,20]. However, our study suggests that with more optimal RF current delivery more optimal energy distribution is possible thus resulting in greater spherical shape of ablation. Indeed, tip exposures <4 cm produced relatively round zones of ablation, with only the electrode tip exposure of 5 cm producing a sphericity index of less than 85%. As the 5 cm tip exposure ablations were associated with reaching the generator current output maximum and a condition where pulsing was not seen we surmise that further gains in sphericity could theoretically be achieved for this electrode as well at even higher currents. Alternatively or concomitantly, greater durations of energy deposition (i.e., longer than 15 min) may be needed for larger tip exposures to create optimal thermal distribution.

Overall, larger electrode tip exposures increased the total amount of heating achieved producing a higher order relationship between total heating and ablation size.

Experimental data produced very tight correlations for both logarithmic and power modeling, and thus further research is likely required to determine which is more predictive. We further observed that maximum temperatures in the ablated tissue increased exponentially with active electrode tip size and attribute this to the greater possible energy deposition achieved with larger tip exposure. Increased maximum temperatures may have also been facilitated by longer ablation times with larger active tips. Regardless, when taken as a whole, our findings suggest that prior results may have been limited by generator output or were less than optimal based upon inefficient energy deposition algorithms. Indeed, we attribute our observation that initial current output had only a modest effect on ablation size with R^2 ranging from 0.40–0.70 to the fact that an optimal energy deposition algorithm can in many circumstances 'self-correct' to match generator output with the maximum energy deposition that can be tolerated by the tissue. The dynamic nature of this process further underscores the fact that such tissue capacity changes over time, likely due to cumulative heating effects of time coupled with changes in the heated tissue volume.

Although our study did demonstrate greater energy deposition and larger tip exposure increases the ablative zone, it further identified that there are deleterious effects of too much energy being applied too rapidly. Indeed, this is true even with a self-regulating system such as the one used in this study as initial currents that were too high resulted in smaller ablation zones. Overall, we noted that an important factor was the time to first pulse. Indeed, we observed that the optimum time to first pulse, for tip exposure greater than 2 cm, was noted to range between 30–120 s. Very short time to first pulse (<30 s) had the greatest negative effect, whereas times longer than 2 min tended to decrease ablation size. This varied from electrode to electrode tip exposure size based on tissue heating characteristics. We attribute these findings to tissue changes surrounding the electrode. If tissue heating occurred too fast (i.e., if the time to initial pulse is too short), there is rapid formation of a sufficient number of gas bubbles forming surrounding the electrode that cannot be cleared during the following cooling cycle, retarding the procedure. Conversely, if the heating was too slow, a penalty of long procedure time with inefficient heating was incurred.

In general, most clinically available internally-cooled electrodes systems have limited the electrode exposure to the 2.5–3 cm range based on less than optimal results or inconsistent results [21]. Our study suggests that electrode size could theoretically be expanded to 4 cm and possibly 5 cm with increased energy in clinical practice.

Another element seen in this study is the relevance of the overall duration of ablation. Utilizing shorter active tips for extended time did not improve diameter (likely as thermal equilibrium was achieved). Thus, our findings suggest that potentially shorter ablation times than reported for many current clinical guidelines could be employed for smaller tip exposures. On the other hand, longer active tips achieved larger ablation diameters only after 12 or even 15 min of heating. This is also logical, as it likely takes longer to achieve equilibrium deeper in the tissue. All in all, given the need for clinical efficiency, our findings point to the need for further evaluation and possible refinement of current clinical algorithms.

Our study further documents the benefits of non-continuous heating including varying the RF pulse and time applied. Additionally, we show that judicious selection of initial current is mandated, as this also drives when pulsing is mandated. Our study confirms previous studies [17] that demonstrate that based upon the non-uniform heat distribution within tissues surrounding an electrode and the maximum temperature limitations of any given tissue prior to vaporization that strategies using a continuous amount of energy will ultimately retard efficient energy propagation.

We acknowledge several limitations of this study. First, it must be noted that we performed this study in an *ex-vivo* model in one tissue type (i.e., *ex-vivo* bovine liver). We note that this is the most common model for studying ablation (and hence enables direct comparison to prior studies) and that the principles of thermal ablation from RF can likely be extended beyond the *ex vivo* liver studied, we readily acknowledge that both an *in-vivo* model to determine effects of perfusion [22], and the study of multiple other clinically relevant tissues will be necessary to determine more precise optimization and quantification. Ultimately, clinical data will likely be needed tailoring algorithms to specific organ sites and tumor types. Additionally, other relevant parameters such as electrode gauge may require further study. Nevertheless, variable algorithm should theoretically permit better matching over a wide range of tissues.

In conclusion, larger reproducible volumes of RF ablation can be achieved due to more efficient delivery and maintenance of the energy deposited into tissue. These findings may have important clinical relevance in regards to the clinical utility of RF ablation compared to other competitive forms of thermal tumor ablation.

Disclosure statement

SNG is a consultant to Cambridge Interventional and Angiodynamics. ERC is owner of Cambridge Interventional. The remaining authors report no conflict of interest.

Funding

This study was financially supported by the Cambridge Interventional.

ORCID

Eliel Ben-David http://orcid.org/0000-0001-7548-5725

References

[1] Hong K, Georgiades C. Radiofrequency ablation: mechanism of action and devices. J Vasc Interv Radiol. 2010;21:S179–S186.

[2] Ahmed M, Solbiati L, Brace CL, et al. Image-guided tumor ablation: standardization of terminology and reporting criteria–a 10-year update. J Vasc Interv Radiol. 2014;25:1691–1705.e4.

[3] Goldberg SN, Gazelle GS. Radiofrequency tissue ablation: physical principles and techniques for increasing coagulation necrosis. Hepatogastroenterology. 2001;48:359–367.
[4] Ikeda K, Osaki Y, Nakanishi H, et al. Recent progress in radiofrequency ablation therapy for hepatocellular carcinoma. Oncology. 2014;87:73–77.
[5] Appelbaum L, Sosna J, Pearson R, et al. Algorithm optimization for multitined radiofrequency ablation: comparative study in *ex vivo* and *in vivo* bovine liver. Radiology. 2010;254:430–440.
[6] McRury ID, Diamond S, Falwell G, et al. The effect of ablation sequence and duration on lesion shape using rapidly pulsed radiofrequency energy through multiple electrodes. J Interv Card Electrophysiol. 2000;4:307–320.
[7] Laeseke PF, Sampson LA, Haemmerich D, et al. Multiple-electrode radiofrequency ablation creates confluent areas of necrosis: *in vivo* porcine liver results. Radiology. 2006;241:116–124.
[8] Brace CL. Radiofrequency and microwave ablation of the liver, lung, kidney, and bone: what are the differences? Curr Probl Diagn Radiol. 2009;38:135–143.
[9] Kim SK, Rhim H, Kim Y-S, et al. Radiofrequency thermal ablation of hepatic tumors: pitfalls and challenges. Abdom Imaging. 2005; 30:727–733.
[10] Goldberg SN. Radiofrequency tumor ablation: principles and techniques. Eur J Ultrasound. 2001;13:129–147.
[11] Gulesserian T, Mahnken AH, Schernthaner R, et al. Comparison of expandable electrodes in percutaneous radiofrequency ablation of renal cell carcinoma. Eur J Radiol. 2006;59:133–139.
[12] Solazzo SA, Ahmed M, Liu Z, et al. High-power generator for radiofrequency ablation: larger electrodes and pulsing algorithms in bovine *ex vivo* and porcine *in vivo* settings. Radiology. 2007; 242:743–750.
[13] Brace CL, Laeseke PF, Sampson LA, et al. Radiofrequency ablation with a high-power generator: device efficacy in an *in vivo* porcine liver model. Int J Hyperthermia. 2007;23:387–394.
[14] Brace CL, Sampson LA, Hinshaw JL, et al. Radiofrequency ablation: simultaneous application of multiple electrodes via switching creates larger, more confluent ablations than sequential application in a large animal model. J Vasc Interv Radiol. 2009;20: 118–124.
[15] Nishikawa H, Kimura T, Kita R, et al. Radiofrequency ablation for hepatocellular carcinoma. Int J Hyperthermia. 2013;29:558–568.
[16] Goldberg SN, Solbiati L, Halpern EF, et al. Variables affecting proper system grounding for radiofrequency ablation in an animal model. J Vasc Interv Radiol. 2000;11:1069–1075.
[17] McGahan JP, Loh S, Boschini FJ, et al. Maximizing parameters for tissue ablation by using an internally cooled electrode. Radiology. 2010;256:397–405.
[18] Goldberg SN, Gazelle GS, Solbiati L, et al. Radiofrequency tissue ablation: increased lesion diameter with a perfusion electrode. Acad Radiol. 1996;3:636–644.
[19] Hoffmann R, Rempp H, Erhard L, et al. Comparison of four microwave ablation devices: an experimental study in *ex vivo* bovine liver. Radiology. 2013;268:89–97.
[20] Abreu L, Damasceno-Ferreira JA, Monteiro ME, et al. Volume and shape assessment of renal radiofrequency ablation lesion. Urology. 2018;116:229.e7–229.e11.
[21] Rempp H, Mezger D, Voigtlaender M, et al. A comparison of internally water-perfused and cryogenically cooled monopolar and bipolar radiofrequency applicators in *ex vivo* liver samples. Acad Radiol. 2014;21:661–666.
[22] Schutt DJ, Haemmerich D. Effects of variation in perfusion rates and of perfusion models in computational models of radio frequency tumor ablation. Med Phys. 2008;35:3462–3470.